

## Inelastic Scattering of Slow Neutrons by Lattice Vibrations in Aluminum\*

R. S. CARTER,† H. PALEVSKY, AND D. J. HUGHES  
*Brookhaven National Laboratory, Upton, New York*

(Received March 12, 1957)

The lattice vibrations of aluminum have been studied by means of the inelastic scattering of "cold" neutrons, in which the neutron absorbs a phonon whose energy is typically much larger than the incident neutron energy. Neutrons with a wavelength about 5 Å were obtained by filtering a beam of thermal neutrons through eight inches of beryllium. After scattering in an aluminum single crystal, the neutron energy distribution was determined by time of flight, using a mechanical chopper. The peaks observed in the energy distribution of the scattered neutrons for various crystal orientations were used to determine the "scattering surface" in a plane parallel to one face of the cubic lattice. The scattering surface gives the dispersion law for the crystal, that is, the frequency,  $\omega$ , of the lattice vibration phonons as a function of the wave vector,  $\mathbf{q}$ . Dispersion curves, obtained for three different directions in the crystal, agree well with x-ray results and with theoretical calculations of the dispersion based on the assumption of harmonic forces.

### I. INTRODUCTION

THE properties of lattice vibrations of crystalline materials were first investigated theoretically in connection with specific heats. In order to account for the observed variation of specific heat with temperature, Debye considered the crystal vibrations as a set of waves traveling in a continuous elastic medium,<sup>1</sup> with a velocity, independent of frequency, determined by the elastic constants of the medium. A more realistic model of the crystal as a set of coupled oscillators was developed later by Born and von Kármán.<sup>2</sup> On the basis of such a crystal model, it is possible in principle to calculate the detailed behavior of the lattice vibrations, with results dependent on the particular interatomic force model used. Thus detailed measurements of the lattice vibration properties can lead to a better understanding of interatomic forces.

Measurements of elastic constants by static or dynamic methods give information on the long-wavelength vibrations only. For these wavelengths, however, the crystal medium is accurately represented by a continuum and the Debye theory holds. In order to observe deviations from the Debye model, which occur in the region where the details of the crystal structure and the interatomic forces become important, it is necessary to observe the behavior of the extremely high-frequency ( $10^{13}$ /sec) vibrations whose wavelengths are of the order of the interatomic spacings. For many years, no direct methods of investigation were available for the interesting high-frequency region of the lattice vibration spectrum. Some information was available from the diffuse scattering of x-rays, and recently this method has been advanced greatly,<sup>3,4</sup> with the

result that dispersion curves have been obtained extending to the frequency limit. With the high neutron fluxes available from nuclear reactors, a new method of great potentiality now becomes possible,<sup>5-9</sup> viz., the study of the large changes in neutron energy and momentum produced by interactions with the lattice vibration phonons. As will be seen below, these large energy and momentum changes offer a more direct and easily interpreted technique than the use of x-rays. The present paper reports preliminary results utilizing long-wavelength or "cold" neutrons, and primarily serves to establish the feasibility of the method; precision results must await the availability of even higher neutron flux than was used in the present apparatus.

### II. THEORY

The theory of the interaction of neutrons with crystal lattices has been developed by several authors,<sup>10-14</sup> of which we shall use the results obtained by Placzek and Van Hove.<sup>14</sup> The energy quantum of an elastic wave, the phonon, is characterized by its energy,  $\hbar\omega$  ( $\omega$ , the angular frequency, rad/sec), which is a function of its wave vector  $\mathbf{q}$  ( $q = 2\pi/\lambda$ , where  $\lambda$  is the wavelength of the vibration). Similarly,  $\mathbf{k}$  represents the neutron wave vector, and the neutron energy is  $\hbar^2 k^2/2m$  where  $m$  is the mass of the neutron. In the usual case of one-phonon scattering, the neutron absorbs or emits one phonon. Conservation of energy requires that  $\hbar^2/2m(k_0^2 - k_f^2) = \hbar\omega$ ; hence

$$k_0^2 - k_f^2 = (2m/\hbar)\omega, \quad (1)$$

<sup>5</sup> B. N. Brockhouse and A. T. Stewart, Phys. Rev. **100**, 756 (1955).

<sup>6</sup> B. N. Brockhouse, Can J. Phys. **33**, 889 (1955).

<sup>7</sup> B. Jacrot, Compt. rend. **240**, 745 (1955).

<sup>8</sup> Carter, Muether, Hughes, and Palevsky, Bull. Am. Phys. Soc. Ser. II, **1**, 55 (1956).

<sup>9</sup> Carter, Hughes, and Palevsky, Phys. Rev. **104**, 271 (1956).

<sup>10</sup> G. C. Wick, Physik. Z. **38**, 403, 689 (1937).

<sup>11</sup> R. Seeger and E. Teller, Phys. Rev. **62**, 37 (1942).

<sup>12</sup> R. Weinstock, Phys. Rev. **65**, 1 (1944).

<sup>13</sup> A. Akhiezer and I. Pomeranchuk, J. Phys. (U.S.S.R.) **11**, 167 (1947).

<sup>14</sup> G. Placzek and L. Van Hove, Phys. Rev. **93**, 1207 (1954).

\* Work performed under contract with the U. S. Atomic Energy Commission.

† Now at Westinghouse Research Laboratories, Pittsburgh, Pennsylvania.

<sup>1</sup> P. Debye, Ann. Physik **39**, 789 (1912).

<sup>2</sup> M. Born and T. von Kármán, Physik. Z. **13**, 297 (1912); **14**, 15 (1913).

<sup>3</sup> E. H. Jacobsen, Phys. Rev. **97**, 654 (1955).

<sup>4</sup> C. B. Walker, Phys. Rev. **103**, 547 (1956). This paper and reference 3 contain references to much of the earlier work on the thermal diffuse scattering of x-rays.

where the subscript 0 refers to the incident neutron and  $f$  to the scattered neutron. Equation (1) must be satisfied for both coherent and incoherent scattering, but for the former, an additional condition holds. When the neutron is scattered coherently, the interference of the scattered waves requires

$$\mathbf{k}_0 - \mathbf{k}_f = \mathbf{q} + 2\pi\boldsymbol{\tau}, \quad (2)$$

where  $\boldsymbol{\tau}$  is an arbitrary vector of the reciprocal lattice. Since  $k$  and  $q$  are proportional to momentum, Eq. (2) can be considered as expressing the conservation of momentum between the neutron, the phonon, and the crystal, with  $\boldsymbol{\tau}$  representing the momentum taken up by the crystal as a whole in the interaction.

Experimental results obtained from incoherent scattering and their interpretation in terms of lattice vibration spectra have already been reported.<sup>6,9</sup> Here we are interested in the more revealing and more complex coherent inelastic scattering. In the case of coherent elastic scattering, in which no phonon is exchanged, Eq. (2) reduces to  $\mathbf{k}_0 - \mathbf{k}_f = 2\pi\boldsymbol{\tau}$ , which is just the Bragg scattering condition. Since  $\omega$  is a function of  $\mathbf{q}$ , Eqs. (1) and (2) can be satisfied simultaneously for only particular values of  $\mathbf{k}_f$ , if one assumes that  $\mathbf{k}_0$  is fixed. The conditions imposed by the vector Eq. (2) are illustrated in Fig. 1. The magnitude of  $k_f$  and  $q$  are uniquely determined by the additional conditions imposed by Eq. (1). As the direction of the incident neutrons,  $\mathbf{k}_0$ , is varied relative to the orientation of the crystal, determined by  $\boldsymbol{\tau}$ , the end point of the vector  $\mathbf{k}_f$  sweeps out the surface  $S$ .  $S$ , which is called the *Scattering surface*, determines the allowed energy for the inelastically scattered neutrons.  $S$  will depend, of course, on the value of  $\mathbf{k}_0$  and on the angle between  $\mathbf{k}_0$  and  $\mathbf{k}_f$ . Since only those neutrons with  $\mathbf{k}_f$  lying on  $S$  will appear in the scattered beam, the energy distribution will show a sharp peak at an energy corresponding to the particular value of  $\mathbf{k}_f$ . In the actual crystal, there will be three modes of propagation of the elastic waves corresponding to the three different types of polarization—two transverse and one longitudinal. Thus, in general there will be three scattering surfaces corresponding to the different types of waves, so the energy distribution of the scattered neutrons should exhibit at least three discrete peaks. Actually, fewer peaks may be observed owing to degeneracy of the transverse modes in particular crystal directions, or more peaks may appear because of complications of the surface, which allow  $\mathbf{k}_f$  to cross the same surface in two or more different points.

The foregoing discussion covers the basic principles of the manner in which experimental results can be used to infer the properties of the lattice vibration phonons. Experimentally, it is only necessary to measure the energy of the peaks in order to determine both  $\mathbf{q}$  and  $\omega(\mathbf{q})$ , utilizing Eqs. (1) and (2). The parameters  $\mathbf{k}$ ,  $\boldsymbol{\tau}$ , and the relative angles are determined by the experimental conditions, i.e., the incident

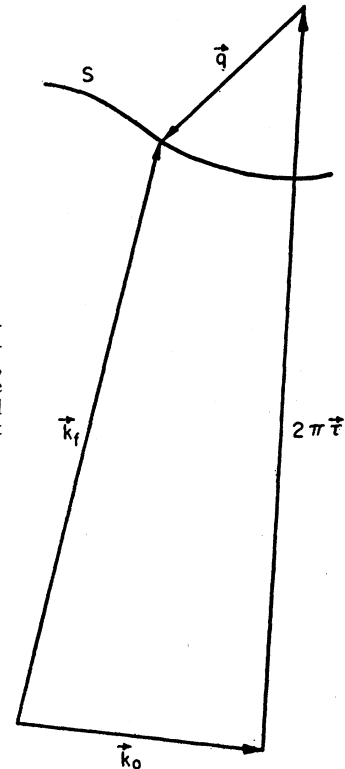


FIG. 1. Vector representation of the conditions expressed by Eq. (2) i.e.,  $\mathbf{k}_0 - \mathbf{k}_f = \mathbf{q} + 2\pi\boldsymbol{\tau}$ .  $S$  is the scattering surface generated by varying  $\mathbf{k}_0$  with respect to  $\boldsymbol{\tau}$ .

energy and the crystal orientation. The energy of the peak gives  $k_f$  directly so that  $\mathbf{q}$  can be determined from the vector diagram in Fig. 1, and  $\omega(\mathbf{q})$  from the conservation of energy, Eq. (1). The function  $\omega(\mathbf{q})$ , the dispersion relation, for the three polarizations, constitutes the fundamental information concerning the lattice vibrations.

In principle, the above discussion applies to x-rays as well as neutrons. The change in the wave vector,  $\mathbf{k}_f - \mathbf{k}_0$ , giving  $\mathbf{q}$ , can be easily determined for x-rays, but the energy of the x-rays is so large compared to the phonon energy that the energy change of the x-rays cannot be determined. Instead,  $\omega(\mathbf{q})$  can be determined only indirectly from the intensity of the thermal diffuse scattering. Thus, the interpretation of x-ray data requires the use of a rather fundamental assumption, and furthermore, the intensity data must be corrected for contributions from Compton scattering and multiple-phonon processes. In addition, results can only be obtained for waves traveling in directions of high symmetry in the crystal, since it is only by suppression of one or more of the modes of polarization that it is possible to separate the contribution of the different types of waves to the intensity. On the other hand, neutrons with the same wavelengths, because of their appreciable mass, are available with energies, as in the present results, much smaller than the phonon energies—so the energy changes can be easily measured. Even multiple-phonon and incoherent processes do not affect the shape of position of the peaks,

but add a continuous background, which is slowly varying with energy so that the one-phonon coherent peaks can easily be identified. As each mode of polarization is represented by a distinct peak, it is not necessary to limit the observations to waves traveling in particular directions in order to separate the different modes of propagation. Thus, the use of neutrons offers a very direct approach, employing only the basic concepts of conservation of energy and momentum and requiring no serious corrections. In spite of the inherent advantages of neutrons over x-rays, the neutron experiments are still in the preliminary stage because of the limited neutron intensities available at present relative to x-ray intensities.

### III. EXPERIMENTAL TECHNIQUE

An aluminum crystal was chosen for investigation because of its low absorption and incoherent cross section, and because large single crystals are easily obtainable. These considerations are important in order to obtain sufficient intensity. Very low-energy or "cold" neutrons from the Brookhaven reactor were used. Although the neutron flux is greater for neutrons nearer thermal energies, their use requires very good energy and angular resolution to obtain significant results. A fairly monochromatic beam was obtained by filtering the neutrons through a polycrystalline beryllium filter. The Be filter, 8 in. thick, was cooled to liquid nitrogen temperatures, its transmission for the long-wavelength neutrons thereby being increased a factor of three. In the filter, only those neutrons with wavelengths greater than 4 Å were transmitted, and the mean transmitted wavelength was 4.7 Å, corresponding to a temperature of 40°K, with a half-width spread of about 15°K, a result of the shape of the neutron energy distribution in the reactor. The effectiveness of the cooled filter was such that the intensity for neutrons with  $\lambda > 4$  Å was a factor of 1000 greater than for neutrons with  $\lambda < 4$  Å. Since the Debye temperature of aluminum is 400°K, the neutron energy gain will be of the order of 300°K, which is large compared to the spread in incident energy.

The experimental arrangement is shown in Fig. 2. The filtered beam, with an angular spread of 3°, is incident on the scattering crystal, at room temperature.

The neutrons scattered at 90° to the incident beam pass through a mechanical chopper, and travel a 4-m flight path to a bank of shielded BF<sub>3</sub> counters, the angular spread of the scattered neutrons being 5°. The energy distribution of the scattered neutrons is determined by standard time-of-flight techniques. Points on the scattering surface are determined for different orientations of the crystal with respect to the fixed directions of the incident and scattered beams. A large, single crystal of aluminum was available in the form of a cylinder 3 in. in diameter and 5 in. long. The large crystal, combined with the filter and chopper technique, allowed a beam with cross-sectional area as

large as 8 sq in. to be used. The incident flux of filtered "cold" neutrons was about 10<sup>6</sup> neutrons per cm<sup>2</sup> per sec, so the total number of neutrons incident on the crystal per sec was about 5 × 10<sup>6</sup>.

The difficulty of the present type of experiment is strikingly illustrated by the fact that because of the very small cross section for inelastic scattering the small solid angle subtended, and the duty cycle of the chopper, only one neutron per sec was scattered into the detector, in spite of the high intensity in the beam emerging from the reactor. Although a ton of shielding was placed around the counter, the rate due to room-background neutrons was about 5 per sec. Fortunately, the inelastically scattered neutrons are concentrated in narrow energy peaks; hence, when their intensity is determined as a function of time, distinct peaks can be seen above the background. The true counting rate in a channel at the peak is about equal to the background counting rate. Since twelve points are taken simultaneously, the large background, being independent of time, does not have to be accurately determined. Being constant, the effect of the large background appears primarily in the large statistical uncertainty it introduces into each point, rather than in any shape distortions. Some typical energy distribution curves are shown in Fig. 3. The flux of neutrons per given wavelength interval,  $d(nv)/d\lambda$ , is shown as a function of  $\lambda$ . The vertical scale is the total number of counts per channel, with background subtracted. The statistical accuracy is indicated by the scatter of the points. It was necessary to overlap three sets of 12 points each

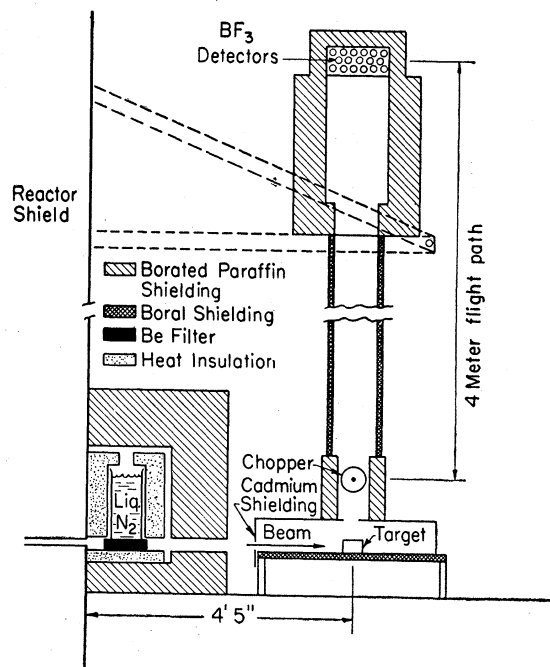


FIG. 2. Schematic diagram of experimental arrangement at the Brookhaven reactor.

in order to cover the whole energy range, and each curve represents about 48 hours running time.

#### IV. ENERGY DISTRIBUTION OF SCATTERED NEUTRONS

Some examples of the peaks present in the various energy distributions of the scattered neutrons are shown in Fig. 3. The location of the peaks are indicated by numbers, which correspond to the numbered points in the experimental scattering surfaces of Fig. 5. The observed width of the peaks is a result of the resolution of the time-of-flight equipment and the spread in the incident neutron energy. The data are shown on a wavelength scale since  $\lambda$  is proportional to the directly measured neutron time-of-flight. On this scale, the time-of-flight resolution is 0.14 Å (full width at half-maximum), and is independent of the neutron wavelength. The contribution of the spread of the incident neutron energy to the resolution width is difficult to determine, as it varies with the orientation of the crystal and the shape of the scattering surface. On the average, the contribution is about equal to that of the time-of-flight equipment, giving a total resolution width of 0.2 Å. The position of the center of the peaks determines  $k_f$ , and this position can be determined to about one-fifth of the resolution width, corresponding to a 4% error in  $k_f$ . This error in  $k_f$  ranges from 0.04 to 0.10 in units of ( $2\pi \text{ Å}^{-1}$ ), whereas the spread in  $k_0$  resulting

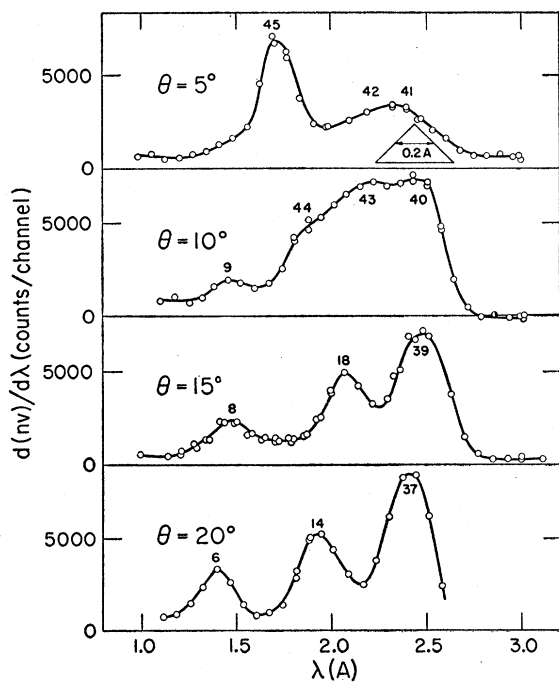


FIG. 3. Energy distribution of the inelastically-scattered neutrons from aluminum for four different orientations of the crystal relative to the incident neutron beam. The numbers indicate the position of the peaks and correspond to the numbered points in Fig. 5. The resolution, shown by the triangle, is constant on a wavelength scale.

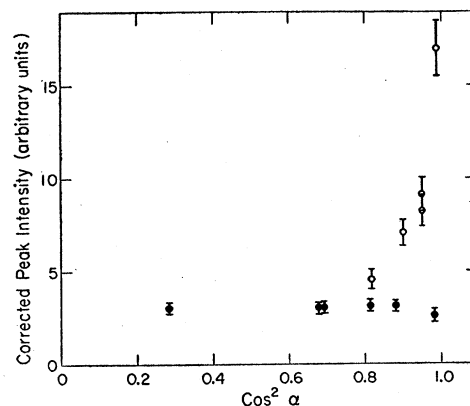


FIG. 4. Dependence of peak intensity upon  $\cos^2 \alpha$ , where  $\alpha$  is the angle between the polarization vector  $\mathbf{e}$  (assumed to have the same direction as  $\mathbf{q}$ ) and the vector  $\mathbf{k}_f - \mathbf{k}_0$ . The intensities have been corrected for all other factors in the theoretical intensity expression. The open circles represent those peaks believed to be due to one-phonon coherent scattering, and the closed circles represent the "anomalous peaks."

from the width of the incident neutron distribution is about 0.16 on the same units.

In a few of the energy distribution curves, a very broad peak of low intensity appeared at unusually high energies. No peak of normal width and magnitude was found at such high energy indicating that the low, broad peaks were due to some other process than one-phonon coherent scattering. It was shown, experimentally, that these "anomalous peaks" were not the result of instrumental or room-background effects, hence they resulted from neutrons scattered from the aluminum crystal. In order to separate this type of scattering from the one-phonon coherent type, the relative intensities of the peaks were studied. The intensity of the one-phonon coherent scattering depends along with other factors, directly on the square of the cosine of the angle,  $\alpha$ , between the phonon polarization vector,  $\mathbf{e}$ , and the vector  $\mathbf{k}_f - \mathbf{k}_0$ .<sup>14</sup> If one assumes that the high-energy peaks result from absorption of longitudinally polarized phonons, the direction of  $\mathbf{q}$  is approximately the same as  $\mathbf{e}$ , and thus the angle  $\alpha$  is known. Figure 4 shows the intensity (after correcting for the other intensity factors) of all the peaks with  $\lambda < 1.6 \text{ Å}$  as a function of  $\cos^2 \alpha$ . The closed circles, those suspected of being "anomalous," show no variation with  $\cos^2 \alpha$ , and, therefore, cannot be due to the one-phonon coherent process. The open circles, representing the normal peaks, show a marked dependence on  $\alpha$ , as expected, although the dependence is not precisely linear. The anomalous peaks were not used in the analysis of lattice vibrations since they did not result from one-phonon coherent scattering. Further work is being planned to identify their source.

#### V. SCATTERING SURFACE

With  $\mathbf{k}_0$  known and  $\mathbf{k}_f$  measured, it is necessary to have only the orientation of the crystal relative to

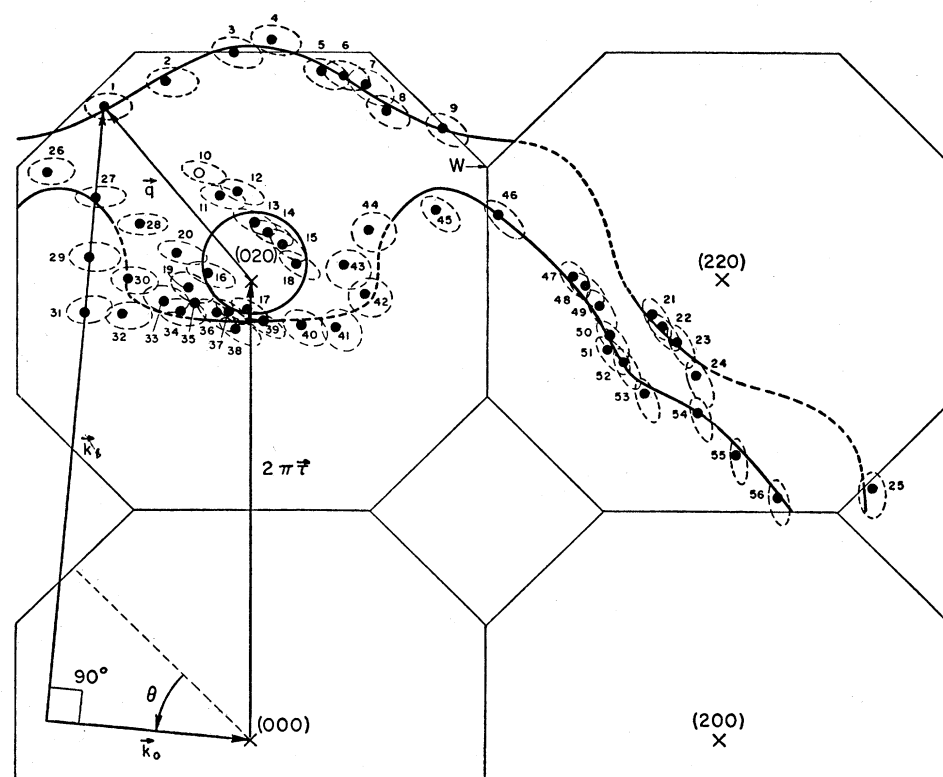


FIG. 5. Scattering surface for aluminum in reciprocal-lattice space. The reciprocal-lattice points, which define the plane, are denoted by crosses. The numbered points are the end points of the measured neutron scattering vectors  $\mathbf{k}_f$  and are numbered to correspond to the peaks in Fig. 3 and the points in the following figures. The errors of the points are shown by the dotted ovals. The heavy solid line is the scattering surface, and the dotted sections show where the data were insufficient to determine the surface. The octagonal pattern defines the Brillouin zones.

$\mathbf{k}_f$  and  $\mathbf{k}_0$ , that is,  $\tau$ , in order to determine the scattering surface. The face-centered cubic aluminum crystal was oriented so that one face of the cubic lattice lay in the plane defined by the directions of the incident and scattered neutrons. In reciprocal lattice space,  $\mathbf{k}_0$  and  $\mathbf{k}_f$  thus lie in the plane containing the (000), (200), and (020) reciprocal-lattice points. Different regions of the scattering surface were investigated by orienting the crystal about an axis perpendicular to this plane. Figure 5 is a diagram of this plane, showing the angle,  $\theta$ , defining the orientation of the crystal relative to  $\mathbf{k}_0$  and  $\mathbf{k}_f$ , and the experimentally determined scattering surface. The angle  $\theta$  was varied in  $5^\circ$  steps until energy distributions had been determined over one quadrant of the diagram. For each value of  $\theta$ , a line was drawn perpendicular to  $\mathbf{k}_0$  and the corresponding value of  $k_f$  obtained from the scattering data used to fix the length of  $\mathbf{k}_f$ . Each end point of  $\mathbf{k}_f$  thus determined is a point on the scattering surface. The points are numbered in order to identify them with the peaks shown in Fig. 3 and with the points on the curves in the next section. The dotted oval around each point delineates the error arising from the various sources already discussed. The regular octagonal pattern defines the boundaries of the Brillouin zones.

The several branches of the surface shown are constructed simply by connecting the points smoothly. In some regions no data could be obtained, and in other regions the errors or the points overlapped so as

to obscure the surface. In these doubtful regions, the dotted line represents a guess at the shape of the surface. That the outer surface is the longitudinal branch is readily determined from the intensity of point 4 at the top of the diagram. If it were on a transverse branch, the factor  $\cos^2\alpha$  would be about zero and the peak would be of very low intensity. Instead, the peak is intense, indicating that  $\cos^2\alpha$  is approximately unity and that the point belongs to the longitudinal branch. The small circle around the (020) reciprocal-lattice point also belongs to the longitudinal branch. Since all the  $q$ 's on this circle are small, it lies in a region of long wavelength where the simple Debye model holds. When one uses the elastic constants for aluminum with the Debye model, a surface very similar to the experimentally determined one results for the longitudinal but not for the transverse branch. Furthermore, the peak represented by the point 13 at the top of the circle has too much intensity to belong to the transverse branch. The remaining surface, that not ascribed to the longitudinal, must correspond to the transverse branch. Actually, there should be two surfaces for the two transverse branches, but they are too similar to be separated with the present resolution.

The surfaces should be symmetric around the (020) and the (220) directions. The open circle, point number 10, thus seems spurious for it has no counterpart on the other side of (020) axis of symmetry, even though

it was well defined in the experimental energy distribution. Calculations based on a simple, assumed relationship between  $\omega$  and  $\mathbf{q}$ , were carried out which showed that it would be possible for the peak to arise entirely from the scattering of incident neutrons with  $k_0$  smaller than the mean value used in the diagram. This possibility was confirmed experimentally by using a narrow-wavelength band determined by two filters, and measuring the difference in the energy distributions. The distribution was first measured with a Be filter with a 4-A cutoff, then with a BeO filter with a 4.67-A cutoff. Subtraction of the two sets of data gave the distribution curve resulting for incident neutrons with  $k_0$  between 1.57 and 1.34 in units of  $2\pi \text{ \AA}^{-1}$ . In this way, the contribution of the lower-energy neutrons ( $k < 1.34$ ) was eliminated. The suspected peak vanished in the difference curve, showing that it was completely due to the low-energy tail. Consequently, it was not used in drawing the scattering surface. The two-filter method improves the resolution and makes interpretation of the data easier and more accurate. It requires much more running time, however, since two sets of data must be taken, each with sufficient statistical accuracy to make the difference between the two sets

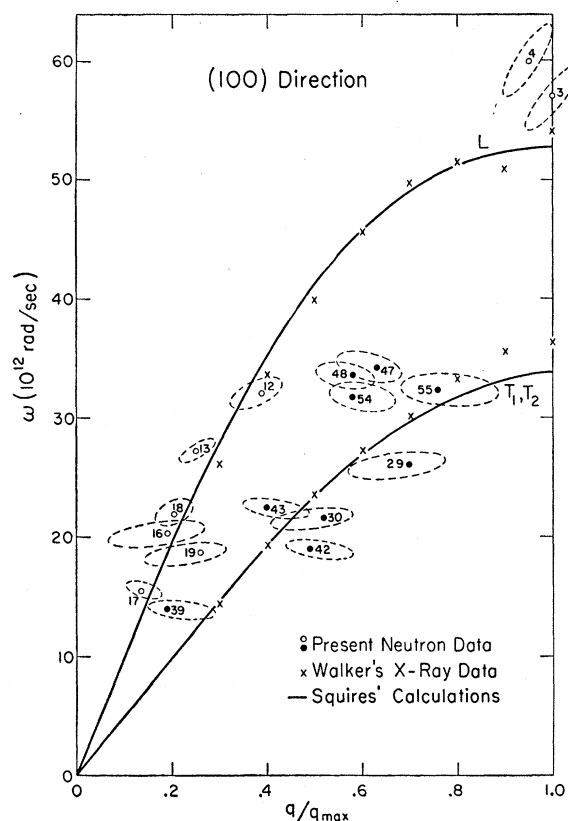


FIG. 6. Dispersion curve for phonons traveling in the (100) direction. The open circles correspond to the longitudinal branch and the closed circles to the transverse branches; the numbers identify the experimental points in Fig. 5. The calculations of Squires<sup>15</sup> and the experimental results of Walker<sup>4</sup> are also shown.

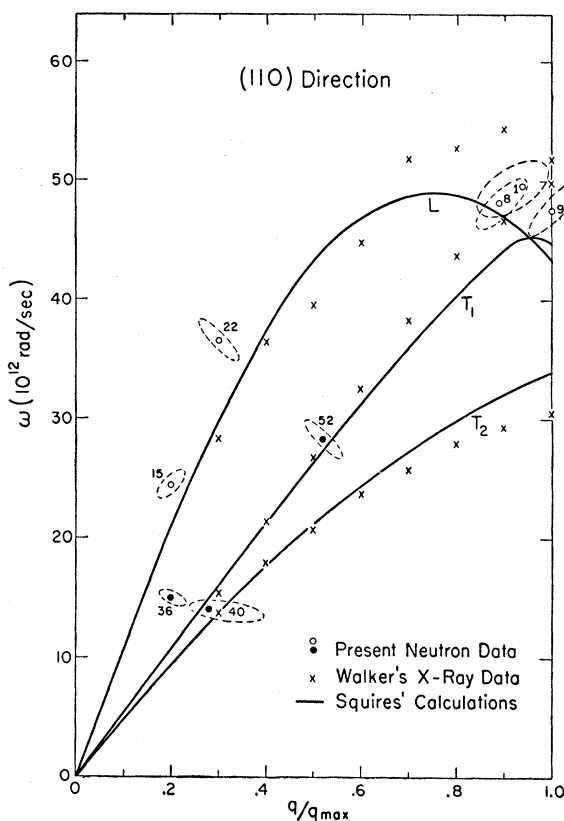


FIG. 7. Dispersion curve for phonons traveling in the (110) direction.

meaningful. The present intensity did not allow the use of this method for all the data taken.

In order to obtain the desired dispersion law,  $\omega$  as a function of  $\mathbf{q}$ , the direction and magnitude of the phonon wave vector,  $\mathbf{q}$ , is read directly from Fig. 5 for any direction of  $\mathbf{q}$ . Its circular frequency  $\omega$  is then determined directly from Eq. (1). As the function  $\omega(\mathbf{q})$  varies with the direction of  $\mathbf{q}$  in the crystal, any plot of  $\omega$  vs  $\mathbf{q}$  must be made using only those points with equivalent directions of  $\mathbf{q}$ . Thus plots were made for  $\mathbf{q}$ 's in the (100), the (110), and the direction of the corners of the Brillouin zone labeled  $W$ . The experimental points lying within  $+8^\circ$  of each direction were used.

The dispersion curves thus obtained are shown in Figs. 6, 7, and 8. Each experimental point is numbered to correspond to Fig. 5, and the errors, shown by the dotted regions, are derived from Fig. 5. The open circles correspond to the longitudinal, and the closed circles to the transverse branch. The solid curves are derived from Squires' calculations on aluminum,<sup>15</sup> in which he assumes that the crystal forces are harmonic and exist only between first- and second-nearest neighbors, thus requiring a total of five force constants. The

<sup>15</sup> G. L. Squires, Phys. Rev. **103**, 304 (1956).

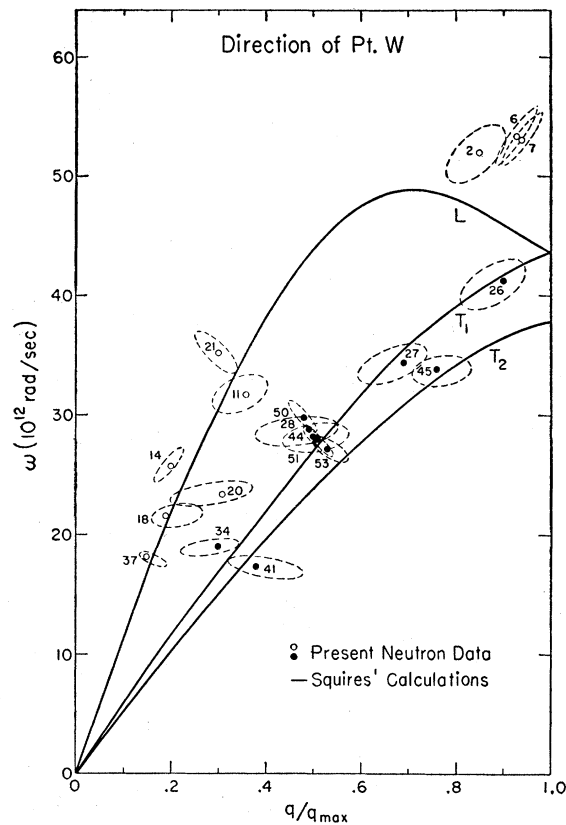


FIG. 8. Dispersion curve for phonons traveling in the direction of the corners of the Brillouin zone labeled *W*. No x-ray data are shown since they cannot be obtained in this direction.

five constants are related to the three well-established elastic constants. In order to determine numerical values for all five constants, however, he chose them to be the best fit to Walker's x-ray data<sup>4</sup> in addition to the measured elastic constants. The  $\times$ 's are Walker's experimental data for the dispersion relation obtained from the diffuse scattering of x-rays.

The neutron data, on the whole, agree well with the calculated curve and the x-ray data. In the (100) direction (Fig. 6), the open circles fit the lower part of the theoretical curve, but indicate that it should be a

little higher at the upper limit. The large scatter of the closed circles does not allow any definite conclusions to be drawn, concerning the transverse branch, but does indicate, as do the x-ray data, that the calculated curve should be higher for large  $q$ . In this direction the two transverse branches,  $T_1$  and  $T_2$ , are degenerate. There are only a few neutron points in the (110) direction (Fig. 7); here the longitudinal branch again agrees quite well with the calculations. The two transverse branches are separated in this direction, but the neutron data are not sufficient to distinguish them. It is not possible to obtain x-ray data for the point *W* direction since the contribution of the several modes to the diffuse x-ray intensity cannot be separated. For neutrons, however, there is no such distinction. The open circles again indicate that the calculated curve should be higher for large  $q$ . The closed circles, however, agree very well with the theoretical curves, although the two branches are not resolved experimentally.

In summary, the neutron data agree fairly well with the x-ray data and the theoretical calculations. Where some difference does appear to exist, however, the present data are not sufficiently accurate or detailed to warrant a re-evaluation of the force constants for aluminum. They indicate that the constants need some modification and possibly that a more detailed model must be used; however, recalculations should await better neutron results. The present work demonstrates the value of the scattering of cold neutrons as a tool for the investigation of lattice vibrations. The accuracy is limited only by the resolution, which at present is handicapped by the available intensity. Since the interpretation of the results is based directly on such fundamental principles as the conservation of energy and momentum, there is no possibility of hidden systematic errors arising out of the necessity of making corrections, or depending on assumptions. Because of the promise of the neutron approach, extensive modifications of the equipment have been made<sup>16</sup> to obtain greater neutron intensity, and work with better resolution is now in progress.

<sup>16</sup> Pelah, Eisenhauer, Hughes, and Palevsky, *Bull. Am. Phys. Soc. Ser. II*, **2**, 43 (1957).